

CO₂ Reduction

Cathodic Hydroxide Ions Induce Tetrose Formation during Glycolaldehyde Electroreduction to Alcohols: A Potential CO₂-to-Carbohydrate Pathway

Ernest Pahuyo Delmo⁺, Haichuan Zhang⁺, Jessa Vispo De Guzman, Rans Miguel Nunag Lintag, Juhee Jang, Yao Yao, Yinuo Wang, Shangqian Zhu, Tiehuai Li, Mingguang Pan, Hongming Xu, King Lun Yeung, and Minhua Shao*

Abstract: The electrochemical synthesis of organic compounds from CO₂ can potentially alleviate climate change by hampering the atmospheric accumulation of greenhouse gases. The production of carbohydrates from CO₂ reduction will have promising applications for the manufacturing of valuable, multi-carbon compounds that are traditionally produced from the petrochemical or agricultural industries. In this work, we analyzed the copper-catalyzed electrochemical reduction of glycolaldehyde, a commonly observed trace CO₂RR product that has been previously proposed as an intermediate for alcohol formation. We determine that glycolaldehyde is not the main intermediate on polycrystalline copper-based electrocatalysts that selectively produce ethanol. In an unbuffered electrolyte, the cathodic hydroxide ions produced induce the coupling of glycolaldehyde to tetroses in the solution phase, yielding a maximum glycolaldehyde-to-sugar conversion of 47.2% under ambient conditions. Using in situ infrared spectroscopy coupled with density functional theory (DFT) calculations, we show that glycolaldehyde reduction to alcohols proceeds via adsorption of its enol tautomer, $\eta^2(\text{C,C})\text{--CHOH=CHOH}$. Our findings not only shed light on the C₂ alcohol formation pathways during CO₂RR, but also imply that a CO₂ electrolyzer can potentially produce C₄ carbohydrates via CO₂ reduction to glycolaldehyde followed by C–C coupling in the solution phase, with only a high local pH needed to drive the tetrose formation step.

Introduction

Electrochemical synthesis technologies have the capacity to overhaul the petroleum-dependent chemical process industries with an energy-efficient and environment-friendly alternative.^[1] Producing valuable organic compounds from CO₂ gas remains the cornerstone of such technologies due to its prospect to simultaneously mitigate atmospheric CO₂ accumulation while providing an efficient energy storage system for intermittent renewable energy sources. To achieve high faradaic efficiencies toward valuable compounds, forming carbon–carbon bonds is an integral step of the electrochemical CO₂ reduction reaction (CO₂RR) mechanism. Multiple pathways have been proposed on the coupling

of various C₁ intermediates (i.e., *CO, *CHO, *COH, and *CH_x) to form C₂ adsorbates on different metal catalysts, which will then subsequently reduce to C₂ hydrocarbons and oxygenates.^[2] In recent years, C–C coupling mechanisms toward C₃ and C₄ compounds have also been demonstrated to be feasible during CO₂RR as well, yielding unconventional C₃₊ organic compounds, such as 1-propanol,^[3–5] 2-propanol,^[6] propylene,^[7–9] propane,^[9,10] methylglyoxal,^[11,12] furandiol,^[11] 1-butanol,^[13,14] and *t*-butanol.^[15] To form these C₃₊ compounds, surface-mediated (heterogeneous) C–C bond formation steps have been proposed, such as *CO + *CH₃CO coupling^[16] and *CH_x insertion.^[9] Homogeneous coupling pathways in the vicinity of the cathode (i.e., in the solution phase) have also been utilized to achieve high C₄


[*] E. P. Delmo⁺, H. Zhang⁺, J. V. De Guzman, R. M. N. Lintag, J. Jang, Y. Yao, Y. Wang, S. Zhu, T. Li, M. Pan, H. Xu, K. L. Yeung, M. Shao
Department of Chemical and Biological Engineering, The Hong Kong University of Science and Technology, Clear Water Bay, Kowloon, Hong Kong, China
E-mail: kemshao@ust.hk


Y. Yao
School of Sciences, Great Bay University, Dongguan 523000, China

M. Shao
Energy Institute, Chinese National Engineering Research Center for Control & Treatment of Heavy Metal Pollution, and CIAC-HKUST Joint Laboratory for Hydrogen Energy, The Hong Kong University of Science and Technology, Clear Water Bay, Kowloon, Hong Kong, China

M. Shao
Guangzhou Key Laboratory of Electrochemical Energy Storage Technologies, Fok Ying Tung Research Institute, The Hong Kong University of Science and Technology, Guangzhou 511458, China

[†] Both authors contributed equally to this work.

 Additional supporting information can be found online in the Supporting Information section

 © 2025 The Author(s). Angewandte Chemie International Edition published by Wiley-VCH GmbH. This is an open access article under the terms of the [Creative Commons Attribution-NonCommercial License](#), which permits use, distribution and reproduction in any medium, provided the original work is properly cited and is not used for commercial purposes.

FEs in recent studies. For instance, the aldol condensation of acetaldehyde (a minor CO₂RR product on copper-based catalysts^[5,17,18]) to crotonaldehyde has allowed for the direct conversion of CO₂ to 1-butanol during electrolysis.^[13,14,19] Aside from acetaldehyde, glycolaldehyde has also been observed as a trace CO₂RR^[5,20–22] and CORR^[23] product on copper-based electrocatalysts. Density functional theory (DFT) calculations have also indicated that adsorbed glycolaldehyde may be a possible intermediate of the ethanol and ethylene glycol pathways on Cu.^[24,25] In our recent work on glyoxal electroreduction,^[26] we hypothesized that the pH-induced aldol reaction of glycolaldehyde may also open up an alternative CO₂-to-C₄ electroreduction pathway.

Aside from simply forming C–C bonds, the reactivity of glycolaldehyde is of broad interest to CO₂RR research because its self-aldol reaction forms higher-order carbohydrates, such as tetroses and/or hexoses, typically in the presence of enzymes, inorganic catalysts, and/or at elevated temperatures/pressures.^[27–30] Furthermore, in the presence of formaldehyde, glycolaldehyde can initiate and catalyze the formose reaction to form higher-order sugars.^[31–33] Achieving an effective artificial CO₂-to-carbohydrate pathway will be a step forward toward realizing global food security, which can have a significant impact in sustainable space exploration.^[31,34–36] Building on this, the proof of concept of a multi-step, abiotic CO₂-to-sugar pathway was recently analyzed by Cestellos-Blanco et al.,^[31] who proposed that electrochemical CO₂RR may be used to synthesize formaldehyde (as already demonstrated in Ref. [37]) and glycolaldehyde. A Ca(OH)₂ catalyst can then be added to the post-electrolysis solution, which, at slightly elevated temperatures, would lead to the production of valuable carbohydrates, such as glucose.^[31] Other carbohydrate formation pathways have also been explored in recent years, such as the electrochemical CO₂ reduction to acetic acid/acetate followed by its conversion to carbohydrates via biotic means,^[38,39] and the electrochemical oxidation of methanol to formaldehyde, which can subsequently be converted to sugars via the formose reaction.^[40] Our previous study, however, showed that sugars may also be produced during glyoxal electroreduction at a high local pH (without the need for elevated temperatures).^[26] With this in mind, we aimed to probe the possible mechanisms behind abiotic sugar formation from CO₂RR by comprehensively analyzing the electrochemical reduction of glycolaldehyde, a commonly observed trace CO₂RR product on copper. We show that glycolaldehyde reduction leads to ethylene glycol, ethanol, and acetaldehyde as the end products, indicating that glycolaldehyde is not the main CO₂RR intermediate for copper-based CO₂RR catalysts that selectively produce ethanol as the sole C₂ alcohol. The reduction process is observed to proceed via the $\eta^2(\text{C,C})\text{--CHOH=CHOH}$ adsorbate, which demonstrates the role of enolization during aldehyde reduction to alcohols. Finally, for the first time, we show that glycolaldehyde conversion to higher-order sugars can occur on a copper cathode in an electrochemical cell under ambient conditions, with only the cathodic hydroxide anions needed to drive the reaction in an unbuffered electrolyte. Our findings imply that it is possible to produce C₄ sugars via glycolaldehyde coupling

in a single-step, locally-alkaline CO₂RR electrolyzer without the need for the succeeding formose reaction step at elevated temperatures.

Results and Discussion

Electrochemical Reduction to Alcohols

In an aqueous solution, the glycolaldehyde dimer dissociates to form monomeric glycolaldehyde, as shown in Figure S1a. Both the aldehyde and diol forms of glycolaldehyde are detectable in the ¹H NMR spectrum, in which the hydrated form was predominant (95.4% abundance based on the $\text{--CH}_2\text{OH}$ normalized area). In the ¹³C NMR spectrum (Figure S2), only hydrated, monomeric glycolaldehyde was detectable. Further magnification of the 3.2 to 6.1 ppm region in the ¹H NMR spectrum (Figure S1b) shows that trace amounts of cyclic and acyclic glycolaldehyde dimers are also in equilibrium with the glycolaldehyde monomer. Contrary to previous studies on the aqueous chemistry of glycolaldehyde,^[41,42] the low degree of glycolaldehyde dimerization can be attributed to the dilute glycolaldehyde concentrations employed in this study, in which oligomers are less likely to form. Because the total normalized peak areas of these oligomers were orders of magnitude lower than that of monomeric glycolaldehyde, it was assumed that the presence of these trace oligomers had a negligible impact on the succeeding experiments on glycolaldehyde reduction.

An electropolished copper cathode was used in this study to analyze glycolaldehyde reduction because it is the only metal that can produce advanced organic compounds (> 2e[−]) during CO₂RR, including multiple C₂ products, such as ethylene, ethanol, glycolaldehyde, acetaldehyde, acetate, and ethylene glycol (as demonstrated in Ref. [5] and Figure S3). Because glycolaldehyde has been observed as a trace product in multiple copper-based electrocatalysts,^[5,20–22] it has been proposed as a reaction intermediate of the C₂ pathway.^[24,25] In agreement with this, the electroreduction of glycolaldehyde on copper yields several major products that are also observed during CO₂RR, such as acetaldehyde (2e[−]), ethylene glycol (2e[−]), ethanol (4e[−]), and hydrogen (2e[−] from H₂O), as shown in Figures 1a and S4. Because of the larger copper surface area used in this study (twice the area as that of our previous study^[26]), we observed that the post-electrolysis solution pH was alkaline (pH ≥ 10) at high current densities. Because a highly alkaline pH can affect the stability of aldehydes^[43] and carbohydrates^[44] in the solution, it was necessary to neutralize the electrolyte by bubbling the solution with CO₂ directly after the reaction. As illustrated in Figure S5, the NMR signals of acetaldehyde and glycolaldehyde were significantly suppressed without immediate CO₂-neutralization.

It was observed that the contribution of hydrogen evolution (FE_{max} = 10.1% at −0.86 V) is much lower than that observed during glyoxal reduction,^[26,46] indicating that glycolaldehyde is more reactive than glyoxal during electrolysis. At −0.56 V, only the two electron reduction products, acetaldehyde (FE = 69.0%) and ethylene glycol

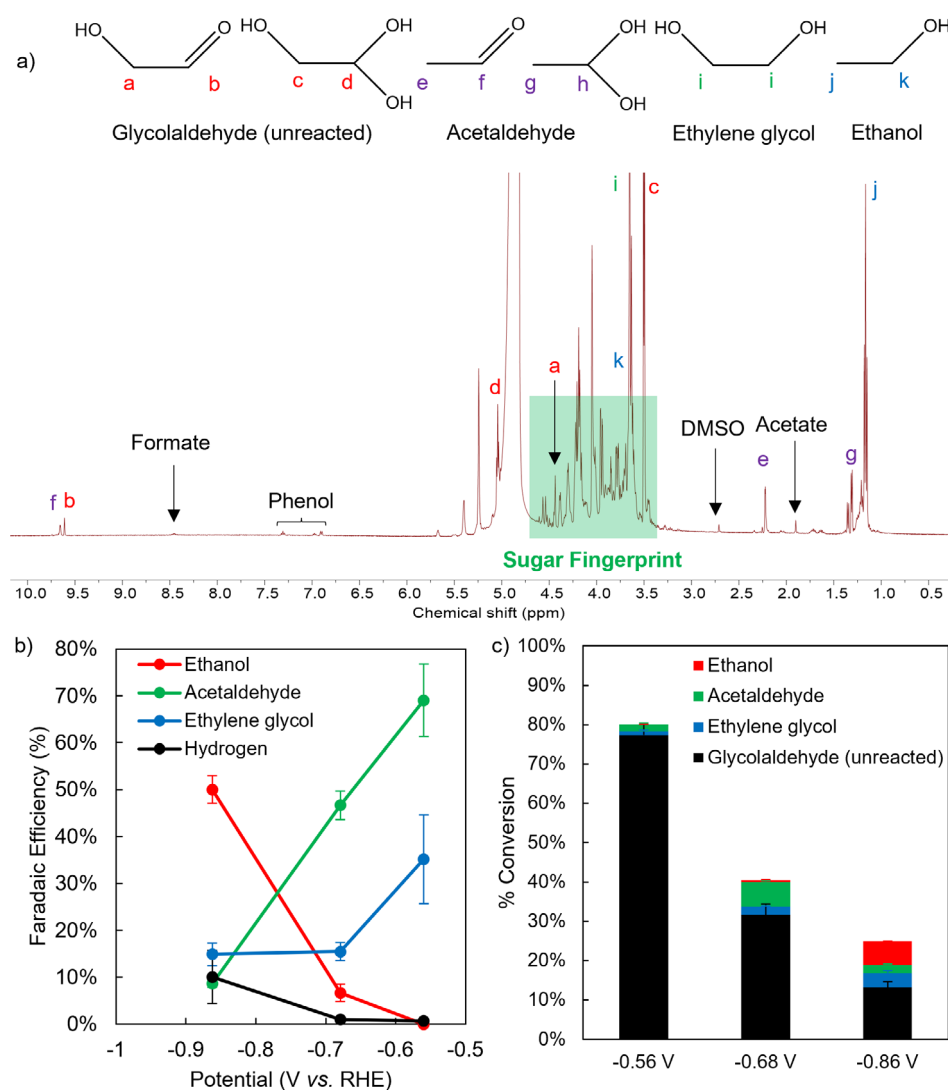


Figure 1. a) Representative ^1H NMR spectrum of the neutralized electrolyte after undergoing glycolaldehyde reduction at -0.86 V (electrolyte: 40 mM glycolaldehyde, 0.1 M KCl). All potentials herein are reported versus the reversible hydrogen electrode (RHE) scale, unless otherwise specified. The spectrum is referenced to the DMSO peak at 2.71 ppm (based on Ref. [45]). b) Faradaic efficiency toward major C_2 products and H_2 gas during glycolaldehyde reduction at various cathodic potentials, c) Percent conversion of glycolaldehyde into various C_2 organics during glycolaldehyde reduction. The error bars are based on the standard deviation of six GC measurements and three ^1H NMR measurements of three independent experiments.

(FE = 35.2%), are readily formed from glycolaldehyde electroreduction. Ethanol formation only occurs at more negative potentials, reaching an FE of 50.0% at -0.86 V. In the study of Schouten et al., glycolaldehyde reduction was observed to lead to ethanol and acetaldehyde as main products using online electrochemical mass spectrometry.^[47] These findings prompted the calculation of CO_2RR pathways with adsorbed glycolaldehyde as an intermediate of ethanol formation.^[24] However, because we observed the significant co-production of ethylene glycol (which, unlike ethanol, is only a trace CO_2RR product on polycrystalline copper^[51]), we concluded that the commonly observed electrochemical CO_2 -to-ethanol pathway on copper that is 1–2 orders of magnitude more selective to ethanol than ethylene glycol does not proceed via glycolaldehyde as an intermediate, as also recently determined by da Silva et al.^[48] As illustrated in Figure

S6, the glycolaldehyde pathway likely diverges from the ethanol-selective pathway early in the C_2 pathway on copper. Although the nature of the exact electrochemical CO_2 -to-ethanol mechanism on Cu is beyond the scope of this work, several ethanol formation pathways that are consistent with our findings (i.e., with glycolaldehyde as a side product but not as an intermediate) have been calculated in literature.^[49,50] These findings are also similar to recent conclusions on the role of glyoxal in the overall CO_2RR mechanism.^[26,46,48] Aside from the main products quantified in Figure 1b, hydrocarbons were also detected in the gas phase, such as ethylene, a major C_2 hydrocarbon produced during Cu-catalyzed CO_2RR . However, because only trace amounts of ethylene (Figure S7) are observed during glycolaldehyde reduction, it can be concluded that glycolaldehyde is not an intermediate of ethylene formation during CO_2RR . Because

ethane ($FE_{\max} = 0.04\%$) and ethylene ($FE_{\max} = 0.02\%$) are produced with similar FEs (Figure S8) as that observed during glyoxal reduction,^[26] it is likely that glycolaldehyde reduction toward these hydrocarbons involves a similar pathway as that of glyoxal reduction.

We further quantified the carbon balance of the system using the C_2 products detected thus far. As shown in Figure 1c, the observed products do not completely account for the total carbon balance, especially at large overpotentials. Because of the transient yellow color observed at all potentials tested (Figure S9), we hypothesized that a majority of glycolaldehyde undergoes C–C coupling, especially at high current densities where a high local pH is achieved. This hypothesis is consistent with our previous findings on glyoxal reduction,^[26] in which these physical indicators were confirmed to be related to C–C coupling processes that form carbohydrates, their decomposition products, and carbon condensates. We then attribute the unaccounted products to a significant side reaction—carbohydrate formation—that occurs alongside glycolaldehyde reduction, as discussed in the succeeding sections.

Production of C_4 Carbohydrates

Even though most of the faradaic current during glycolaldehyde reduction has been accounted for in the C_2 products observed (Figure 1b), a significant amount of carbon has not yet been quantified (Figure 1c), indicating that glycolaldehyde likely undergoes a non-electrochemical side reaction in the electrochemical cell. Indeed, several peaks in the “sugar fingerprint region” at 3.5–4.5 ppm (as also observed in the formose reaction study of Cestellos-Blanco et al.^[31]) are detectable in the post-electrolysis 1H NMR spectra (Figure 1a). Upon analyzing the anomeric proton region of the NMR spectra (Figure 2a), we found that the strong NMR peaks at 5.24 and 5.40 ppm matched the standard anomeric proton peaks of α -threofuranose and β -threofuranose (Figure S10), respectively, indicating that threose is the main sugar formed from C–C coupling via glycolaldehyde aldol reactions. The 5.24 ppm peak exhibits a shoulder, which likely indicates that the furanose forms of erythrose are also present in the solution.^[51,52] Due to the presence of multiple peaks in the sugar fingerprint region of the NMR spectra, it is impractical to deconvolute this region to quantify the carbohydrates produced; therefore, HPLC was instead employed to accurately quantify the tetrose concentrations of the liquid samples. As shown in Figure 2b, the HPLC-RI peaks at 13.16, 13.93, 14.47, and 14.81 min matched the retention times of threose, erythrose, erythrulose, and glycolaldehyde (Figures S11 and S12), respectively, which is consistent with the HPLC data of Barsøe et al.^[42] To ensure the accuracy of the carbohydrate quantification, we further verified that the other components of the electrolyte (e.g., C_2 products, K^+ salts) do not elute in this region (Figure S13). The calculated percent conversions and selectivities toward the tetrose sugars at various cathodic potentials are summarized in Figure 2c. A maximum glycolaldehyde conversion of 47.2% toward tetroses was observed after

a 35-minute electrolysis at -0.86 V, with threose (30.0% conversion) being the preferred C_4 sugar product. To the best of our knowledge, these results provide the first conclusive evidence that significant amounts of sugars can be produced from glycolaldehyde coupling via aldol addition reactions in the electrochemical cell during electroreduction under ambient conditions.

The formation of C_4 sugars from glycolaldehyde is a base-catalyzed aldol addition reaction, which is likely induced by the continuous production of hydroxide anions on the cathode surface. Neither crotonaldehyde nor 1-butanol, which are products of acetaldehyde aldol condensation and subsequent electroreduction, were detectable in the post-electrolysis solution (Figure S14), indicating that no aldol reaction occurs after glycolaldehyde gets reduced to acetaldehyde. The production of hydroxide ions and the resulting aldol addition reaction rate on the cathode are controlled by both the current density (Figure 2c) and the electrolyte buffer capacity (Figure 2d). The low sugar production rate (12.6% conversion) observed at -0.56 V can be attributed to the low current density of 1.6 mA cm^{-2} at this potential (Figure S15). The sharp increase in sugar production at -0.68 V (41.4% conversion, 60.5% selectivity, Figure 2c) is caused by the significant increase in current density to 8.7 mA cm^{-2} at this potential (Figure S15), which causes a fast OH^- production rate. At the same potential, however, the sugar production is significantly inhibited at stronger electrolyte buffer capacities, as shown in Figure 2d. In the 10 mM PPB, 90 mM KCl electrolyte, only an 11.4% glycolaldehyde-to-tetrose conversion is achieved. This highlights the importance of an unbuffered electrolyte in allowing the hydroxide anions produced on the catalyst surface to increase the cathodic pH. Although the conversion increased to 47.2% as the applied potential became more negative at -0.86 V, a decrease in glycolaldehyde-to-tetrose selectivity to 54.4% was also observed. We attributed this to the possible decomposition of sugars at strongly alkaline conditions.^[44] To confirm this, we prepared a 40 mM glycolaldehyde solution in 0.1 M KOH. Within 1 h of sonication, a clear, yellow-colored solution was formed (Figure S16), confirming the formation of sugars. The 1H NMR spectrum of the alkaline solution (Figure S17), however, exhibits only a weak sugar signal in the anomeric proton region. The strong signals of formate ($\delta = 8.43$ ppm), glycolate ($\delta = 3.92$ ppm), and acetate ($\delta = 1.90$ ppm), indicate that the carbohydrates rapidly decompose in strongly alkaline media, as further discussed in Supplementary Note 1 and Figures S18 and S19.

Unlike formose reaction-derived sugars (e.g., glucose, fructose, ribose) that can be metabolized by microorganisms after purification,^[31] the biological significance of glycolaldehyde-derived tetroses remains unexplored due to their high costs and scarcity in nature. We proceeded to investigate whether *Escherichia coli* cells can multiply using standard D-erythrose as the sole nutrient source, as also done by Cestellos-Blanco et al. for formaldehyde-derived sugars.^[31] Unfortunately, it is evident in Figure S20a that, unlike glucose, erythrose cannot sustain *E. coli* growth. After 24 h of exposure in erythrose (Figure S20b), only a negligible number of bacterial colonies remained. Furthermore, the 1H NMR

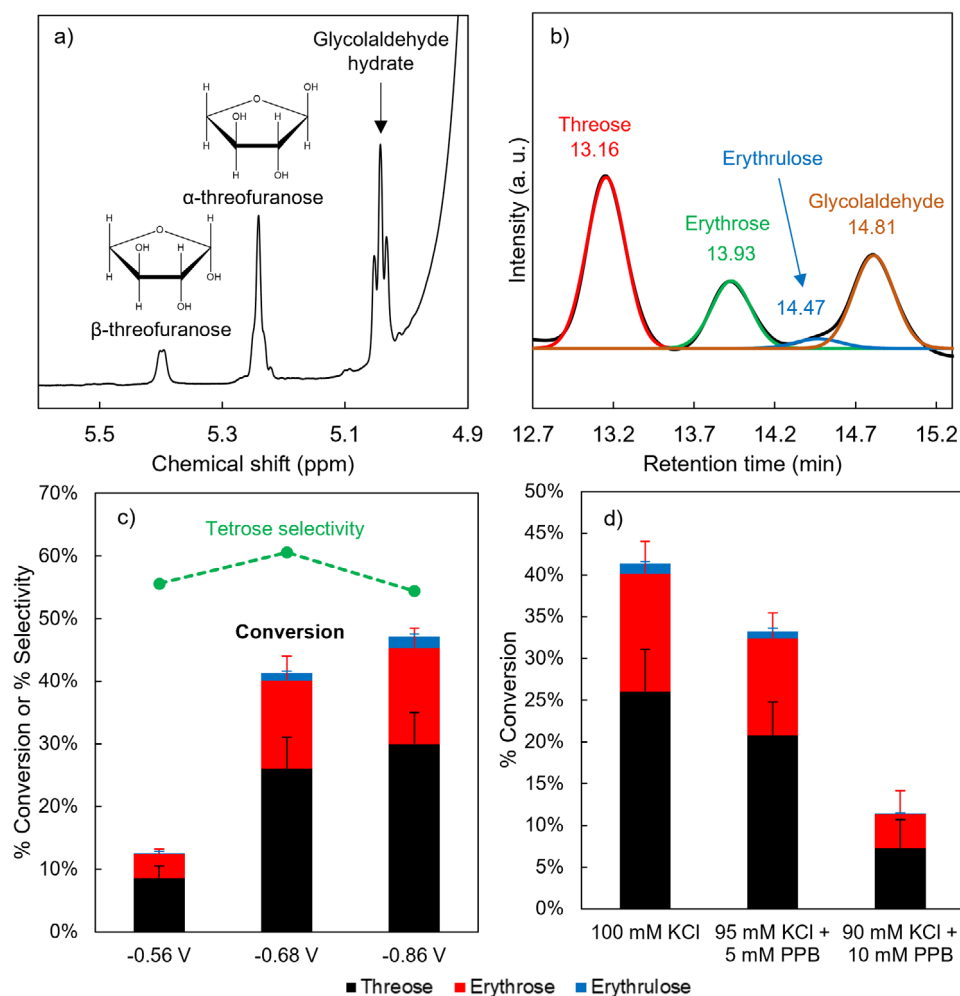


Figure 2. a) Magnified ^1H NMR spectrum of the neutralized electrolyte after glycolaldehyde reduction at -0.68 V in 0.1 M KCl. The anomeric protons of α -threofuranose and β -threofuranose are observed. b) Representative HPLC-RI chromatograph of the neutralized post-electrolysis liquid sample after glycolaldehyde electroreduction at -0.86 V in 0.1 M KCl. c) Percent conversion and selectivity of glycolaldehyde to C_4 sugars (erythrose, threose, and erythrulose) in 0.1 M KCl at various cathodic potentials. The selectivity is defined as the fraction of glycolaldehyde consumed that is converted to tetrose sugars. d) Percent glycolaldehyde-to-tetrose conversion at -0.67 V at varying concentrations of potassium phosphate buffer ([PPB], $\text{pH} \sim 7$). The error bars reflect the standard deviation of three independent experiments.

spectra (Figure S20c) before and after exhibited a negligible decrease in the erythrose concentration of the electrolyte. These results indicate that the metabolism of tetroses by bacteria is not straightforward. This could be because tetroses do not completely convert to cyclic furanoses in solution, and the acyclic aldehydes have been previously demonstrated to be toxic to organisms.^[53,54] Even though specific organisms can consume these sugars,^[55,56] these tetrose molecules may need to be upgraded to hexoses via further aldol reactions before they can be digested by common organisms. However, aside from being a nutrient source, these tetrose molecules, if produced in an inexpensive and sustainable pathway, may also have applications in the pharmaceutical, biomass, and synthetic organic chemical industries.^[52,57]

Mechanism Study of Glycolaldehyde Reduction

Upon establishing all the products observed during glycolaldehyde electrolysis, we further analyzed the interfacial

phenomena that occur during glycolaldehyde reduction via in situ attenuated total reflection-surface enhanced infrared absorption spectroscopy (ATR-SEIRAS) on an electrodeposited copper thin film, which our group has already extensively studied for probing the CO_2RR mechanism on Cu.^[58,59] The 1490 to 1900 cm^{-1} region of the SEIRAS spectra in D_2O at varying potentials during glycolaldehyde reduction is shown in Figure 3a. A deuterated electrolyte was used to study this region to eliminate the contribution of the $\delta(\text{H}-\text{O}-\text{H})$ band at $\sim 1600\text{--}1618\text{ cm}^{-1}$,^[59] as further discussed in Supplementary Note 2 and Figure S21. The negative band at $\sim 1708\text{ cm}^{-1}$ is assigned to the $\nu(\text{C}=\text{O})$ band of solution glycolaldehyde, in agreement with the FTIR spectrum of aqueous glycolaldehyde (Figure S22). The onset of this band, which is attributed to glycolaldehyde consumption, occurred at -0.35 V, in agreement with the observed onset potential of glycolaldehyde reduction via online mass spectrometry data of Schouten et al.^[47] As glycolaldehyde consumption was observed, a positive band

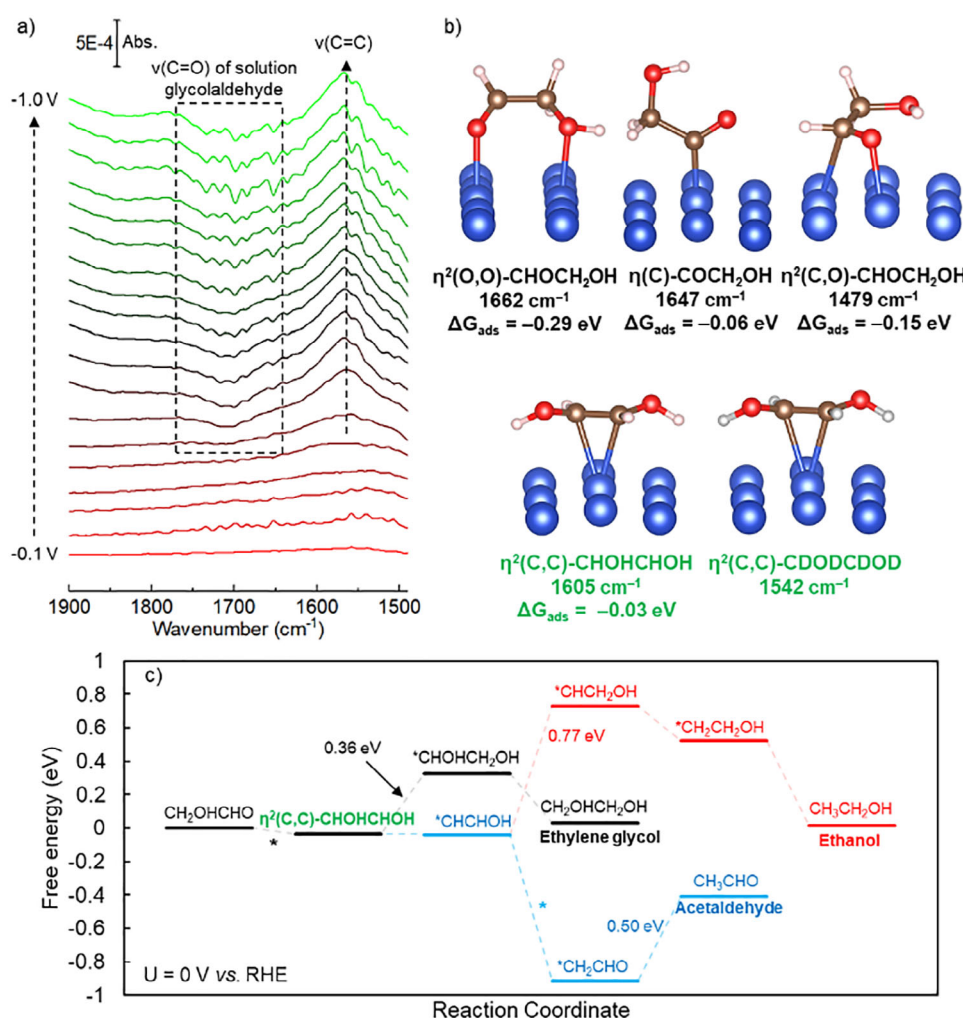


Figure 3. a) In situ ATR-SEIRAS spectra of the Cu thin film (1490 to 1900 cm⁻¹ region) at various cathodic potentials during glycolaldehyde reduction (electrolyte: 40 mM glycolaldehyde, 0.1 M KCl in D₂O). The spectrum at 0 V was used as the reference spectrum. b) Calculated vibrational frequencies (ν(C=O), ν(C=O), or ν(C=C)) and ΔG_{ads} of various possible configurations of adsorbed glycolaldehyde. c) Free energy diagram of glycolaldehyde reduction through the η²(C,C)-CHOH=CHOH intermediate to form ethylene glycol, acetaldehyde, and ethanol. The steps marked with asterisks (*) involve keto-enol tautomerization steps that do not contain proton/electron transfers. The potential-determining steps for the three pathways are labeled. The free energies are referenced to free glycolaldehyde (* + CH₂OHCHO).

emerged at 1567 cm⁻¹, which was attributed to the adsorbed form of glycolaldehyde generated during electroreduction.

To shed light on the nature of adsorbed glycolaldehyde observed in the in situ SEIRAS results, we simulated multiple adsorption configurations using DFT calculations, as illustrated in Figure 3b, based on previously proposed aldehyde adsorption mechanisms. For instance, glycolaldehyde may adsorb on the copper surface via its oxygen atoms (e.g., η²(O,O)-CHOCH₂OH), as also calculated by Garza et al.^[24] Dehydrogenative adsorption of glycolaldehyde may occur to form η(C)-COCH₂OH (2-hydroxyacetyl),^[60] as also proposed during acetaldehyde electroreduction.^[16] However, it can be observed that the observed adsorbate band at 1567 cm⁻¹ does not match the calculated ν(C=O) band of both oxygen-bound (1662 cm⁻¹) and carbon-bound (1647 cm⁻¹) configurations of adsorbed glycolaldehyde on copper. As illustrated in Figure S23, the frequencies still do not match even for a fully deuterated adsorbate nor for other less-

preferred oxygen-bound configurations, indicating that the C=O double bond is not fully intact once glycolaldehyde chemisorbs onto the surface. This may occur through the adsorption of both carbon and oxygen atoms of the carbonyl group to the copper surface, as also suggested previously for acetaldehyde reduction to ethanol.^[16] However, even though the C=O bond strength is significantly reduced for the η²(C,O)-CHOCH₂OH configuration, the redshifted ν(C=O) band of 1479 cm⁻¹ is still inconsistent with our experimental IR data.

Because the observed band is adjacent to the previously observed ν(C=C) bands of adsorbed ethylene^[61] and vinyl alcohol^[62] on copper, we then hypothesized that the 1567 cm⁻¹ band may be the ν(C=C) band of 1,2-ethenediol, an intermediate of aldol coupling that is produced via glycolaldehyde keto-enol tautomerization. As recently observed by Cui et al. using in situ vibrational spectroscopy, acetaldehyde electroreduction can proceed via adsorbed vinyl alcohol (the

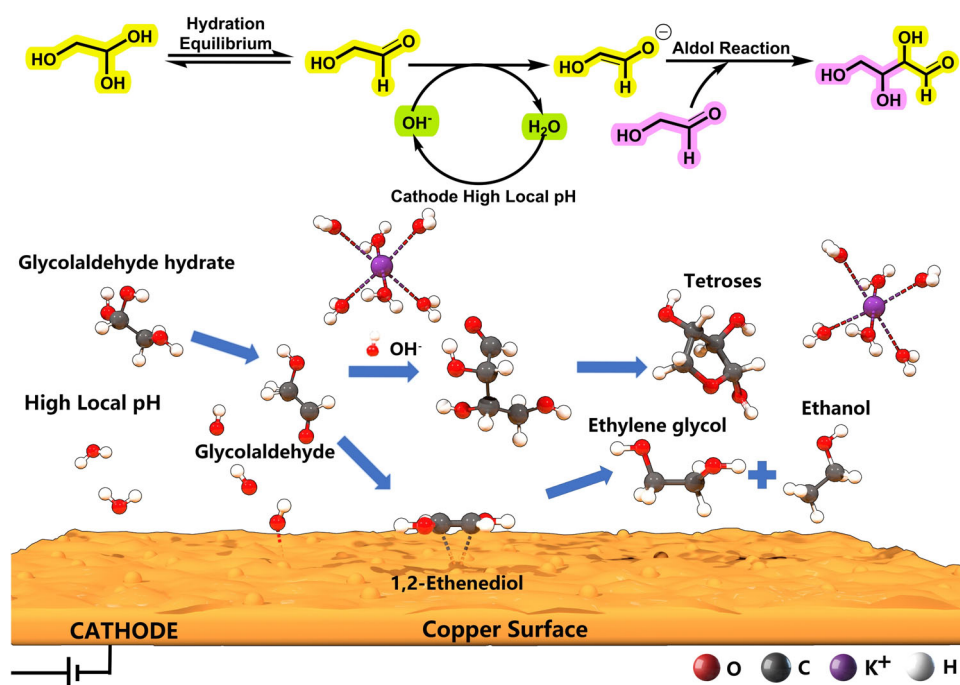


Figure 4. Proposed reaction mechanism toward the formation of alcohols and tetrose sugars during glycolaldehyde electrolysis. Alcohols form through the heterogeneous electrochemical reduction of glycolaldehyde via the $\eta^2(\text{C,C})\text{--CHOH=CHOH}$ adsorbate. Tetroses, such as threose and erythrose, are produced from the aldol addition reaction of glycolaldehyde induced by the high local pH on the copper cathode surface.

enol tautomer of acetaldehyde), with a characteristic $\nu(\text{C=C})$ band at 1522 cm^{-1} .^[62] Our observation of ethane and ethylene formation during glycolaldehyde reduction (Figure S8), albeit at trace amounts, is another indicator of enol adsorption on copper.^[62] Upon simulating the adsorption of 1,2-ethenediol on copper, a theoretical $\nu(\text{C=C})$ vibrational frequency of 1605 cm^{-1} (1542 cm^{-1} if fully deuterated) was calculated for the most stable configuration ($\eta^2(\text{C,C})\text{--CHOH=CHOH}$), which is in close agreement with our experimental data. We therefore concluded that the $\nu(\text{C=C})$ band originates from the adsorption of 1,2-ethenediol, indicating that enolization is not only necessary for aldol coupling, but also plays a role in the adsorption of intermediates during electrochemical reduction. Additional details of our simulations of the possible configurations of 1,2-ethenediol are included in Supplementary Note 3 and Figure S24.

The later stage intermediates of 1,2-ethenediol conversion (whether by electroreduction or aldol coupling) are expected to only exhibit strong $\nu(\text{C--O})$ bands in the $1000\text{--}1100\text{ cm}^{-1}$ wavenumber region, as illustrated in the ex situ IR spectra of aqueous ethylene glycol (Figure S25a) and D-erythrose (Figure S25b), respectively. An analysis of this wavenumber region during in situ SEIRAS is beyond the scope of this work due to the multiple possible C–O–H groups present in the system during alcohol and carbohydrate formation and the strong IR absorption by the Si prism in this region.^[63]

We proceeded to simulate the possible electrochemical pathways of glycolaldehyde electrolysis via 1,2-ethenediol to form ethylene glycol, acetaldehyde, and ethanol, as shown in Figure 3c. The calculated pathways herein are distinct from our previous simulations on the copper-catalyzed glyoxal

electroreduction pathways,^[26] mainly because glyoxal, unlike glycolaldehyde, does not undergo enolization.^[64] It can be observed that the calculated potential-determining steps (PDS) for ethylene glycol and acetaldehyde formation are only 0.36 and 0.50 eV, respectively. These low thermodynamic barriers are consistent with observed high ethylene glycol and acetaldehyde FEs observed even at a low applied potential of -0.56 V . On the other hand, the ethanol pathway has a PDS of 0.77 eV for the reduction of *CHCHOH to $\text{*CHCH}_2\text{OH}$. The large thermodynamic free energy change of this step hinders the formation of ethanol at more positive potentials, which is consistent with our experimental data in which ethanol formation only reaches a significant FE at -0.86 V . As discussed previously, because ethanol formation is significantly preferred over ethylene glycol during CO_2RR on copper-based catalysts, the CO_2 -to-ethanol pathway in these materials likely does not pass through the *CHCHOH adsorbate that forms during glycolaldehyde reduction.

Insights on the CO_2RR Pathways toward Alcohol and Possible Carbohydrate Formation

The proposed reaction scheme toward the formation of alcohols and C_4 compounds via the glycolaldehyde pathway is summarized in Figure 4. On the copper surface, glycolaldehyde first adsorbs as $\eta^2(\text{C,C})\text{--CHOH=CHOH}$ via keto-enol tautomerization, which then gets further reduced to ethanol and ethylene glycol. This mechanism supports multiple simulations that show enol-like species as key precursors toward C_2 alcohols and aldehydes.^[24,50,62] However,

because ethanol production is not orders of magnitude larger than ethylene glycol during glycolaldehyde electroreduction (unlike what is commonly observed during Cu-catalyzed CO₂RR, as demonstrated in Figure S3 and Ref. [5]), we conclude that glycolaldehyde is not the main intermediate toward the ethanol-selective pathway on most copper-based catalysts.

In the solution phase near the cathode surface, we show that the conversion of glycolaldehyde to C₄ sugars can be achieved in an electrochemical cell under ambient conditions, with only a high local pH needed to drive the aldol addition reaction. Unlike the formose reaction, which typically requires a divalent metal catalyst, an elevated temperature, and an organic initiator, the glycolaldehyde-to-tetrose pathway can be realized in reaction conditions that are commonly observed during the electrochemical CO₂ reduction reaction. We therefore propose that a CO₂ electrolyzer can selectively produce C₄ carbohydrates if (1) a high glycolaldehyde faradaic efficiency and local concentration are achieved, and (2) a high local pH can effectively promote the C–C coupling of glycolaldehyde in the solution phase via aldol addition reactions. For the first requirement, the local glycolaldehyde concentrations during CO₂RR are likely to be significantly lower compared to our system. It should be noted, however, that at lower glycolaldehyde concentrations, tetrose formation can still be achieved (Figure S26), albeit at lower conversions (16.5% conversion in a solution containing 10 mM glycolaldehyde). Additionally, a high aldehyde concentration can be achieved locally even though only a trace concentration is detected in the bulk, as demonstrated by Clark and Bell^[65] using DEMS. Therefore, a high glycolaldehyde local concentration can likely be achieved on electrocatalysts that can produce ethylene glycol with glycolaldehyde as a possible intermediate, such as in Ref. [11]. The second requirement for tetrose formation, which is a high local pH during CO₂RR, can likely be attained in a flow cell electrolyzer at high current densities where dissolution of CO₂ into the electrolyte is not needed. It is further noted that the bulk electrolyte in such a flow cell must not be strongly alkaline to prevent the decomposition of the carbohydrates in the liquid phase once they are formed. Otherwise, immediate neutralization of the liquid products is necessary to detect and extract the carbohydrates produced.

Conclusion

This work aimed to unravel the electrochemical pathways of copper-catalyzed glycolaldehyde reduction and reveal its connection to the overall electrochemical CO₂ reduction reaction mechanism. We find that ethylene glycol, acetaldehyde, and ethanol are the main products of glycolaldehyde reduction. The observed potential-dependent product distribution indicates that glycolaldehyde is unlikely to be the key intermediate for most polycrystalline copper-based catalysts that can only selectively produce ethanol. By combining in situ infrared spectroscopy with DFT calculations, we show that glycolaldehyde adsorption occurs through the $\eta^2(\text{C,C})\text{--CHOH=CHOH}$ adsorbate, highlighting the signif-

icance of enol tautomerization during the electroreduction of aldehydes. Finally, for the first time, we observed that the aldol reaction of glycolaldehyde to form tetroses can occur in the electrochemical cell under ambient conditions due to the hydroxide anions produced on the cathode, reaching a maximum conversion of 47.2% in a traditional H-type cell with an unbuffered electrolyte. We hypothesize that the glycolaldehyde pathway, if accessed via CO₂ reduction, can lead to the direct production of C₄ carbohydrates if a high local pH along with a high glycolaldehyde local concentration are achieved.

Supporting Information

The authors have cited additional references within the Supporting Information.^[5,13,14,26,41,42,44,45,51,52,58,59,62,66–87]

Author Contributions

E.P.D. and M.S. conceptualized and designed the experiments for the project. E.P.D. performed all electrochemical reduction and in situ ATR-SEIRAS experiments. H.Z. performed all the DFT calculations. J.V.D.G. and R.M.N.L. performed the bacterial growth experiments. E.P.D., H.Z., Y.Y., S.Z., and H.X. analyzed the in situ ATR-SEIRAS results. E.P.D., H.Z., J.J., Y.Y., Y.W., T.L., and M.P. performed and analyzed the GC and NMR experiments. E.P.D., H.Z., and Y.W. performed and analyzed the HPLC experiments. M.S. and K.L.Y. supervised the project and acquired funding for the project. All authors contributed to the writing and editing of the manuscript.

Acknowledgements

This work was supported by the Research Grants Council (16310419, 16304821, 16308420, and JLFS/P-602/24), the Guangzhou Science and Technology Bureau (2024A03J0609), the Innovation and Technology Commission via the Chinese National Engineering Research Center for Control & Treatment of Heavy Metal Pollution, and Hong Kong Branch of the National Precious Metals Material Engineering Research Center of the Hong Kong Special Administrative Region.

Conflict of Interests

The authors declare no conflict of interest.

Data Availability Statement

The data that support the findings of this study are available from the corresponding author upon reasonable request.

Keywords: Carbohydrate • CO₂ reduction • Electrocatalysis • Glycolaldehyde • Tetrose

- [1] C. Tang, Y. Zheng, M. Jaroniec, S. Qiao, *Angew. Chem. Int. Ed.* **2021**, *60*, 19572–19590.
- [2] S. Nitopi, E. Bertheussen, S. B. Scott, X. Liu, A. K. Engstfeld, S. Horch, B. Seger, I. E. L. Stephens, K. Chan, C. Hahn, J. K. Nørskov, T. F. Jaramillo, I. Chorkendorff, *Chem. Rev.* **2019**, *119*, 7610–7672.
- [3] R. A. Geioushy, M. M. Khaled, K. Alhooshani, A. S. Hakeem, A. Rinaldi, *Electrochim. Acta.* **2017**, *245*, 456–462.
- [4] D. Ren, N. T. Wong, A. D. Handoko, Y. Huang, B. S. Yeo, *J. Phys. Chem. Lett.* **2016**, *7*, 20–24.
- [5] K. P. Kuhl, E. R. Cave, D. N. Abram, T. F. Jaramillo, *Energy Environ. Sci.* **2012**, *5*, 7050–7059.
- [6] A. V. Rayer, E. Reid, A. Kataria, I. Luz, S. J. Thompson, M. Lail, J. Zhou, M. Soukri, *J. CO₂ Util.* **2020**, *39*, 101159.
- [7] J. Gao, A. Bahmanpour, O. Kröcher, S. M. Zakeeruddin, D. Ren, M. Grätzel, *Nat. Chem.* **2023**, *15*, 705–713.
- [8] G. O. Larrazábal, V. Okatenko, I. Chorkendorff, R. Buonsanti, B. Seger, *ACS Appl. Mater. Interfaces.* **2022**, *14*, 7779–7787.
- [9] Y. Zhou, A. J. Martín, F. Dattila, S. Xi, N. López, J. Pérez-Ramírez, B. S. Yeo, *Nat. Catal.* **2022**, *5*, 545–554.
- [10] M. Esmailirad, Z. Jiang, A. M. Harzandi, A. Kondori, M. T. Saray, C. U. Segre, R. Shahbazian-Yassar, A. M. Rappe, M. Asadi, *Nat. Energy.* **2023**, *8*, 891–900.
- [11] K. U. D. Calvino, A. W. Alherz, K. M. K. Yap, A. B. Laursen, S. Hwang, Z. J. L. Bare, Z. Clifford, C. B. Musgrave, G. C. Dismukes, *J. Am. Chem. Soc.* **2021**, *143*, 21275–21285.
- [12] Y. Li, K. U. D. Calvino, M. Dhiman, A. B. Laursen, H. Gu, D. Santorelli, Z. Clifford, G. C. Dismukes, *EES Catal.* **2024**, *2*, 823–833.
- [13] L. R. L. Ting, R. García-Muelas, A. J. Martín, F. L. P. Veenstra, S. T. Chen, Y. Peng, E. Y. X. Per, S. Pablo-García, N. López, J. Pérez-Ramírez, B. S. Yeo, *Angew. Chem. Int. Ed.* **2020**, *59*, 21072–21079.
- [14] M. Choi, S. Bong, J. W. Kim, J. Lee, *ACS Energy Lett.* **2021**, *6*, 2090–2095.
- [15] M. Kim, J. Park, Y. Choi, H. C. Song, S. Kim, K. Bang, H. C. Ham, N. Kim, D. H. Won, B. K. Min, S. J. Yoo, W. Kim, *Adv. Energy Mater.* **2023**, *13*, 2300749.
- [16] X. Chang, A. Malkani, X. Yang, B. Xu, *J. Am. Chem. Soc.* **2020**, *142*, 2975–2983.
- [17] Y. Hori, I. Takahashi, O. Koga, N. Hoshi, *J. Phys. Chem. B.* **2002**, *106*, 15–17.
- [18] Y. Hori, I. Takahashi, O. Koga, N. Hoshi, *J. Mol. Catal. A Chem.* **2003**, *199*, 39–47.
- [19] S. P. Cronin, S. Dulovic, J. A. Lawrence, K. A. Filsinger, A. P. Hernandez-Gonzalez, R. Evans, J. W. Stiles, J. Morris, I. Pelczar, A. B. Bocarsly, *J. Am. Chem. Soc.* **2023**, *145*, 6762–6772.
- [20] A. Loiudice, P. Lobaccaro, E. A. Kamali, T. Thao, B. H. Huang, J. W. Ager, R. Buonsanti, *Angew. Chem. Int. Ed.* **2016**, *55*, 5789–5792.
- [21] E. P. Delmo, Y. Wang, J. Wang, S. Zhu, T. Li, X. Qin, Y. Tian, Q. Zhao, J. Jang, Y. Wang, M. Gu, L. Zhang, M. Shao, *Chin. J. Catal.* **2022**, *43*, 1687–1696.
- [22] D. Kim, C. S. Kley, Y. Li, P. Yang, *Proc. Natl. Acad. Sci. USA* **2017**, *114*, 10560–10565.
- [23] J. Hou, X. Chang, J. Li, B. Xu, Q. Lu, *J. Am. Chem. Soc.* **2022**, *144*, 22202–22211.
- [24] A. J. Garza, A. T. Bell, M. Head-Gordon, *ACS Catal.* **2018**, *8*, 1490–1499.
- [25] L. Chen, C. Tang, K. Davey, Y. Zheng, Y. Jiao, S. Qiao, *Chem. Sci.* **2021**, *12*, 8079–8087.
- [26] E. P. Delmo, Y. Wang, S. Zhu, T. Li, Y. Wang, J. Jang, Q. Zhao, A. P. Roxas, G. S. Nambafu, Z. Luo, L. Weng, M. Shao, *J. Phys. Chem. C.* **2023**, *127*, 4496–4510.
- [27] A. Szekrenyi, X. Garrabou, T. Parella, J. Joglar, J. Bujons, P. Clapés, *Nat. Chem.* **2015**, *7*, 724–729.
- [28] X. Garrabou, J. A. Castillo, C. Guérard-Hélaine, T. Parella, J. Joglar, M. Lemaire, P. Clapés, *Angew. Chem. Int. Ed.* **2009**, *48*, 5521–5525.
- [29] H. Kishida, F. Jin, X. Yan, T. Moriya, H. Enomoto, *Carbohydr. Res.* **2006**, *341*, 2619–2623.
- [30] S. Tolborg, I. Sádaba, S. Shunmugavel, S. Meier, P. Fristrup, E. Taarning, presented at 18th International Zeolite Conference: Zeolites for a Sustainable World, Rio de Janeiro, Brazil, 23 Jun **2016**.
- [31] S. Cestellos-Blanco, S. Louisia, M. B. Ross, Y. Li, N. E. Soland, T. C. Detomasi, J. N. C. Spradlin, D. K. Nomura, P. Yang, *Joule* **2022**, *6*, 2304–2323.
- [32] D. Kopetzki, M. Antonietti, *New J. Chem.* **2011**, *35*, 1787–1794.
- [33] O. Pestunova, A. Simonov, V. Snytnikov, V. Stoyanovsky, V. Parmon, *Adv. Space Res.* **2005**, *36*, 214–219.
- [34] N. J. H. Aversch, A. J. Berliner, S. N. Nangle, S. Zezulka, G. L. Vengerova, D. Ho, C. A. Casale, B. A. E. Lehner, J. E. Snyder, K. B. Clark, L. R. Dartnell, C. S. Criddle, A. P. Arkin, *Nat. Commun.* **2023**, *14*, 2311.
- [35] J. B. G. Martínez, K. A. Alvarado, X. Christodoulou, D. C. Denkenberger, *J. CO₂ Util.* **2021**, *53*, 101726.
- [36] C. P. O'Brien, M. J. Watson, A. W. Dowling, *ACS Energy Lett.* **2022**, *7*, 3509–3523.
- [37] K. Nakata, T. Ozaki, C. Terashima, A. Fujishima, Y. Einaga, *Angew. Chem. Int. Ed.* **2014**, *53*, 871–874.
- [38] T. Zheng, M. Zhang, L. Wu, S. Guo, X. Liu, J. Zhao, W. Xue, J. Li, C. Liu, X. Li, Q. Jiang, J. Bao, J. Zeng, T. Yu, C. Xia, *Nat. Catal.* **2022**, *5*, 388–396.
- [39] E. C. Hann, S. Overa, M. Harland-Dunaway, A. F. Narvaez, D. N. Le, M. L. Orozco-Cárdenas, F. Jiao, R. E. Jinkerson, *Nat. Food.* **2022**, *3*, 461–471.
- [40] N. E. Soland, I. Roh, W. Huynh, P. Yang, *ACS Sustainable Chem. Eng.* **2023**, *11*, 12478–12483.
- [41] J. Kua, M. M. Galloway, K. D. Millage, J. E. Avila, D. O. De Haan, *J. Phys. Chem. A.* **2013**, *117*, 2997–3008.
- [42] L. R. Barsøe, S. Saravanamurugan, E. Taarning, J. S. M. Espin, S. Meier, *ChemCatChem.* **2021**, *13*, 5141–5147.
- [43] E. Bertheussen, A. Verdager-Casadevall, D. Ravasio, J. H. Montoya, D. B. Trimarco, C. Roy, S. Meier, J. Wendland, J. K. Nørskov, I. E. L. Stephens, I. Chorkendorff, *Angew. Chem. Int. Ed.* **2016**, *55*, 1450–1454.
- [44] J. M. De Bruijn, A. P. G. Kieboom, H. van Bekkum, *Recl. Trav. Chim. Pays-Bas.* **1986**, *105*, 176–183.
- [45] T. Chatterjee, E. Boutin, M. Robert, *Dalton Trans.* **2020**, *49*, 4257–4265.
- [46] A. M. Reichert, O. Piqué, W. A. Parada, I. Katsounaros, F. Calle-Vallejo, *Chem. Sci.* **2022**, *13*, 11205–11214.
- [47] K. J. P. Schouten, Y. Kwon, C. J. M. van der Ham, Z. Qin, M. T. M. Koper, *Chem. Sci.* **2011**, *2*, 1902.
- [48] A. H. M. da Silva, G. Karaiskakis, R. E. Vos, M. T. M. Koper, *J. Am. Chem. Soc.* **2023**, *145*, 15343–15352.
- [49] F. Calle-Vallejo, M. T. M. Koper, *Angew. Chem. Int. Ed.* **2013**, *52*, 7282–7285.
- [50] T. Cheng, H. Xiao, W. A. Goddard, *Proc. Natl. Acad. Sci. USA* **2017**, *114*, 1795–1800.
- [51] D. S. Wishart, C. Knox, A. C. Guo, R. Eisner, N. Young, B. Gautam, D. D. Hau, N. Psychogios, E. Dong, S. Bouatra, R. Mandal, I. Sinelnikov, J. Xia, L. Jia, J. A. Cruz, E. Lim, C. A. Sobsey, S. Shrivastava, P. Huang, P. Liu, L. Fang, J. Peng, R. Fradette, D. Cheng, D. Tzur, M. Clements, A. Lewis, A. De Souza, A. Zuniga, M. Dawe, et al., *Nucleic Acids Res.* **2009**, *37*, D603–D610.
- [52] S. Tolborg, S. Meier, S. Saravanamurugan, P. Fristrup, E. Taarning, I. Sádaba, *ChemSusChem* **2016**, *9*, 3054–3061.

- [53] L. Benov, I. Fridovich, *J. Biol. Chem.* **1998**, 273, 25741–25744.
- [54] R. M. LoPachin, T. Gavin, *Chem. Res. Toxicol.* **2014**, 27, 1081–1091.
- [55] G. F. Domagk, B. L. Horecker, *Arch. Biochem. Biophys.* **1965**, 109, 342–349.
- [56] H. H. Hiatt, B. L. Horecker, *J. Bacteriol.* **1956**, 71, 649–654.
- [57] Y. N. Palai, A. Fukuoka, A. Shrotri, *ChemCatChem*. **2023**, 15, e202300766.
- [58] E. P. Delmo, Y. Wang, Y. Song, S. Zhu, H. Zhang, H. Xu, T. Li, J. Jang, Y. Kwon, Y. Wang, M. Shao, *J. Am. Chem. Soc.* **2024**, 146, 1935–1945.
- [59] S. Zhu, B. Jiang, W. Cai, M. Shao, *J. Am. Chem. Soc.* **2017**, 139, 15664–15667.
- [60] J. Schnaidt, M. Heinen, Z. Jusys, R. J. Behm, *J. Phys. Chem. C*. **2013**, 117, 12689–12701.
- [61] D. Yamazaki, M. Okada, F. C. Franco Jr, T. Kasai, *Surf. Sci.* **2011**, 605, 934–940.
- [62] Z. Cui, X. Dong, S. G. Cho, M. N. Tegomoh, W. Dai, F. Dong, A. C. Co, *Nat. Commun.* **2022**, 13, 5840.
- [63] X. Liu, P. Zhao, F. Liu, R. Lin, H. Yao, S. Zhu, *J. Energy Chem.* **2024**, 99, 495–511.
- [64] A. R. Fratzke, P. J. Reilly, *Int. J. Chem. Kinet.* **1986**, 18, 757–773.
- [65] E. L. Clark, A. T. Bell, *J. Am. Chem. Soc.* **2018**, 140, 7012–7020.
- [66] M. Dunwell, Y. Yan, B. Xu, *ACS Catal.* **2017**, 7, 5410–5419.
- [67] G. Kresse, J. Furthmüller, *Phys. Rev. B*. **1996**, 54, 11169–11186.
- [68] P. E. Blöchl, *Phys. Rev. B*. **1994**, 50, 17953–17979.
- [69] J. P. Perdew, J. A. Chevary, S. H. Vosko, K. A. Jackson, M. R. Pederson, D. J. Singh, C. Fiolhais, *Phys. Rev. B*. **1992**, 46, 6671–6687.
- [70] A. H. Larsen, J. J. Mortensen, J. Blomqvist, I. E. Castelli, R. Christensen, M. Dulak, J. Friis, M. N. Groves, B. Hammer, C. Hargus, *J. Phys. Condens. Matter*. **2017**, 29, 273002.
- [71] S. Grimme, J. Antony, S. Ehrlich, H. Krieg, *J. Chem. Phys.* **2010**, 132, 154104.
- [72] V. Wang, N. Xu, J. Liu, G. Tang, W. Geng, *Comput. Phys. Commun.* **2021**, 267, 108033.
- [73] A. A. Peterson, F. Abild-Pedersen, F. Studt, J. Rossmeisl, J. K. Nørskov, *Energy Environ. Sci.* **2010**, 3, 1311–1315.
- [74] S. J. Angyal, R. G. Wheen, *Aust. J. Chem.* **1980**, 33, 1001–1011.
- [75] A. Omran, C. Menor-Salvan, G. Springsteen, M. Pasek, *Life*. **2020**, 10, 125.
- [76] Y. Kwon, S. C. S. Lai, P. Rodriguez, M. T. M. Koper, *J. Am. Chem. Soc.* **2011**, 133, 6914–6917.
- [77] M. Dusselier, P. Van Wouwe, F. de Clippel, J. Dijkmans, D. W. Gammon, B. F. Sels, *ChemCatChem*. **2013**, 5, 569–575.
- [78] Z. Zhang, T. Wang, Y. Cai, X. Li, J. Ye, Y. Zhou, N. Tian, Z. Zhou, S. Sun, *Nat. Catal.* **2024**, 7, 807–817.
- [79] Y. Wang, S. Zheng, W. Yang, R. Zhou, Q. He, P. Radjenovic, J. Dong, S. Li, J. Zheng, Z. Yang, G. Attard, F. Pan, Z. Tian, J. Li, *Nature* **2021**, 600, 81–85.
- [80] H. Michelsen, P. Klaboe, *J. Mol. Struct.* **1969**, 4, 293–302.
- [81] G. Socrates, *Infrared and Raman Characteristic Group Frequencies: Tables and Charts, Third edn.*, John Wiley & Sons Ltd, West Sussex, England **2001**.
- [82] V. A. Yaylayan, S. Harty-Majors, A. A. Ismail, *Carbohydr. Res.* **1998**, 309, 31–38.
- [83] M. Osawa, K. Ataka, K. Yoshii, Y. Nishikawa, *Appl. Spectrosc.* **1993**, 47, 1497–1502.
- [84] C. G. P. M. Bernardo, J. A. N. F. Gomes, *J. Mol. Struct.: THEOCHEM* **2001**, 542, 263–271.
- [85] G. T. Merklin, P. R. Griffiths, *J. Phys. Chem. B*. **1997**, 101, 5810–5813.
- [86] I. Villegas, M. J. Weaver, *J. Am. Chem. Soc.* **1996**, 118, 458–466.
- [87] Y. Guo, C. Cai, Y. Zhang, *AIP Adv.* **2018**, 8, 055308.

Manuscript received: March 05, 2025

Revised manuscript received: March 30, 2025

Accepted manuscript online: April 03, 2025

Version of record online: April 17, 2025